CO_2 Capture

DOI: 10.1002/anie.201202176

Polyamine-Tethered Porous Polymer Networks for Carbon Dioxide Capture from Flue Gas**

*Weigang Lu, Julian P. Sculley, Daqiang Yuan, Rajamani Krishna, Zhangwen Wei, and Hong-Cai Zhou**

One of the most pressing environmental concerns of our age is the escalating level of atmospheric CO_2, which is largely correlated to the combustion of fossil fuels. For the foreseeable future, however, it seems that the ever-growing energy demand will most likely necessitate the consumption of these indispensable sources of energy. Carbon capture and sequestration (CCS), a process to separate CO_2 from the flue gas of coal-fired power plants and then store it underground, has been proposed to reduce the anthropogenic CO_2 emissions. Current CO_2 capture processes employed in power plants worldwide are post-combustion "wet scrubbing" methods involving the chemical adsorption of CO_2 by amine solutions such as monoethanolamine (MEA). The formation of carbamate from two MEA molecules and one CO_2 molecule endows the scrubber with a high capacity and selectivity for CO_2. However, this process suffers from a series of inherent problems, such as high regeneration costs that arise from heating the solution (ca. 30% of the power produced by the plant), fouling of the equipment, and solvent boil-off.[1]

To sidestep the huge energy demand, corrosion problem, and other limitations of traditional wet scrubbers, intensive efforts have been made to investigate the use of solid adsorbents as an alternative approach.[2] Compared to wet scrubbing, in which a large amount of water (70% w/w) must be heated and cooled during the regeneration of the dissolved amines, the solid adsorbent approach has the tremendous advantage of improving the energy efficiency of the regeneration process by eliminating the need to heat water.

Porous materials, such as MOF-210,[3] NU-100,[4] and PPN-4,[5] have been deemed to be viable storage alternatives because of their high porosity and, therefore, significantly increased accessible contact area with gas molecules. This could be advantageous because separation and regeneration could be performed under relatively mild conditions compared to amine wet scrubbing systems. Unfortunately, the record high storage capacities do not translate to high selectivities and only moderate CO_2-uptake capacities were observed under carbon capture conditions.

The polarizability and large quadrupole moment of CO_2 can be taken advantage of by introducing CO_2-philic moieties that create strong interactions between the material surface and the CO_2. This will improve the loading capacities and selectivity of CO_2 over other gases. Indeed, this approach has already been proven to be very successful in enhancing the enthalpy of CO_2 adsorption,[6] which can be calculated from CO_2 sorption isotherms at different temperatures and used to quantify the interaction between the material and CO_2. It is worth pointing out that the porosity of the material will be compromised by the introduction of functional groups. CO_2 loading capacities at ambient conditions are dependent on the adsorption enthalpy and porosity (both surface area and pore volume), which must be balanced to achieve high loading.

Besides the loading capacity, another important factor when quantifying how well a material will perform is CO_2 selectivity over N_2. Taking amine scrubbing as the model, aminated porous materials that have been synthesized usually exhibit very large adsorption enthalpies for CO_2 and high CO_2/N_2 selectivities. Recently, Long and co-workers demonstrated the incorporation of *N,N*-dimethylethylenediamine (mmen) at exposed metal centers of CuBTTri (H_3BTTri = 1,3,5-tri(1*H*-1,2,3-triazol-4-yl)benzene), with the new compound mmen-CuBTTri showing drastic enhancement of CO_2 uptake at low pressure, as well as CO_2/N_2 selectivity. It has the highest heat of adsorption for CO_2 (96 kJ mol^{-1}) and one of the highest CO_2/N_2 adsorption selectivities ($S_{IAST} = 327$ at 25 °C) reported to date.[7] Despite its large isosteric heat of CO_2 adsorption, mmen-CuBTTri could easily be regenerated at 60 °C.

It is always important to keep physicochemical stability in mind for practical applications. Purely organic porous polymers are a class of adsorbents that exhibit surface areas comparable to those of metal–organic frameworks (MOFs), but have much higher physicochemical stability because of the entirely covalently bonded network.[6a,8]

The key to obtaining porous polymers with high amine loading is to judiciously select efficient reactions and starting materials with ultrahigh surface areas. PPN-6[9] (PPN stands for porous polymer networks), which has an exceptionally high surface area and an extremely robust all-carbon scaffold

[*] Dr. W. Lu, J. P. Sculley, Z. Wei, Prof. Dr. H.-C. Zhou
Department of Chemistry, Texas A&M University
College Station, TX 77842 (USA)
E-mail: zhou@mail.chem.tamu.edu
Homepage: http://www.chem.tamu.edu/rgroup/zhou/
Prof. Dr. D. Yuan
Fujian Institute of Research on the Structure of Matter Chinese Academy of Sciences
Fuzhou, 350002 (P.R. China)
Prof. Dr. R. Krishna
Van't Hoff Institute for Molecular Sciences
University of Amsterdam
Science Park 904, 1098 XH Amsterdam (The Netherlands)

[**] This work was supported by the U.S. Department of Energy (DOE DE-SC0001015 and DE-AR0000073) and the Welch Foundation (A-1725). We acknowledge Dr. Vladimir Bakhmoutov for his help with solid-state NMR spectroscopy.

Supporting information for this article is available on the WWW under http://dx.doi.org/10.1002/anie.201202176.

based on biphenyl rings, is ideal for the introduction of CO_2-philic groups under harsh reaction conditions. PPN-6 (also known as PAF-1, first reported by Ben et al.[8a]) was synthesized by using a modified Yamamoto homocoupling polymerization procedure.[10] It has a Brunauer–Emmett–Teller (BET) surface area as high as 4023 $m^2 g^{-1}$, and takes up 1.3 mmol g^{-1} (5.4 wt%) CO_2 at 295 K and 1 bar. The polyamine-tethered PPNs (Scheme 1, and see Experimental Section) show dramatic increases in CO_2-uptake capacities at low pressures, and exceptionally high CO_2/N_2 adsorption selectivities under ambient conditions.

Nitrogen gas adsorption/desorption isotherms were collected at 77 K (Figure 1a). The calculated BET surface areas were 1740, 1014, 663, 634, and 555 $m^2 g^{-1}$ for PPN-6-CH_2Cl, PPN-6-CH_2EDA, PPN-6-CH_2TAEA, PPN-6-CH_2TETA, and PPN-6-CH_2DETA respectively. Notably, the huge adsorption/desorption hysteresis in PPN-6-CH_2Cl disappeared into a nearly type I isotherm for the polyamine-tethered PPNs. Along with the decrease in surface area, the pores are smaller after tethering, which supports the reaction occurring within the cavities (see Figure S4 in the Supporting Information).

The efficiency of amine substitution was confirmed by elemental analysis (see Table S5 in the Supporting Informa-

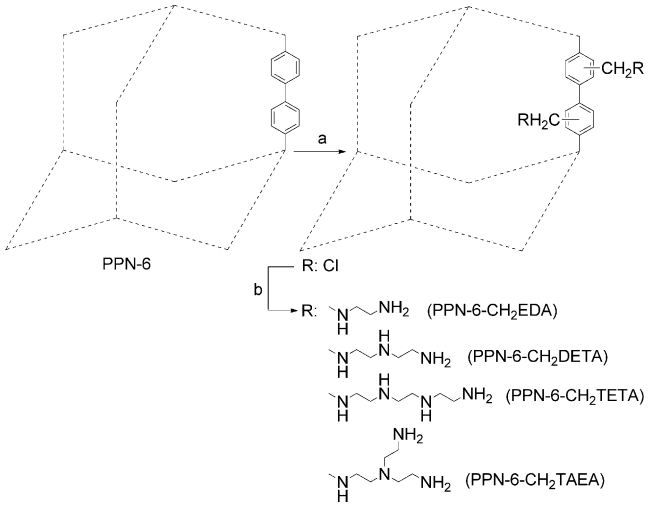

Scheme 1. Synthetic route to polyamine-tethered PPNs. a) $CH_3COOH/HCl/H_3PO_4/HCHO$, 90 °C, 3 days; b) amine, 90 °C, 3 days.

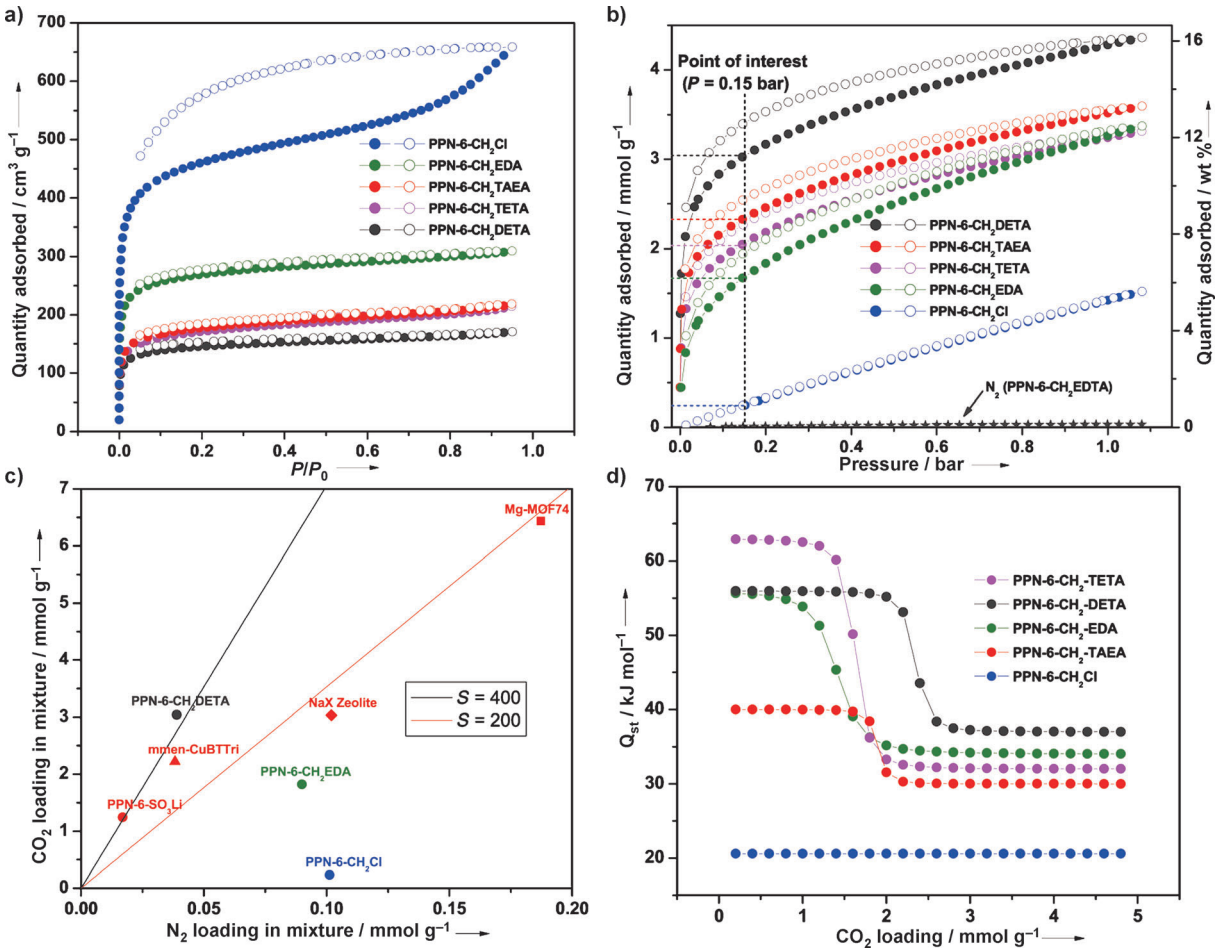

Figure 1. a) N_2 adsorption (●) and desorption (○) isotherms at 77 K. b) CO_2 adsorption (●) and desorption (○) isotherms, as well as PPN-6-CH_2DETA N_2 adsorption, at 295 K. c) The component loadings of N_2 and CO_2 calculated by IAST with bulk gas-phase partial pressures of 85 kPa and 15 kPa for N_2 and CO_2, respectively, with PPN-6-CH_2DETA, PPN-6-CH_2EDA, PPN-6-CH_2Cl, PPN-6-SO_3Li,[9] NaX zeolite,[9] MgMOF-74,[10] mmen-CuBTTri.[7] Loadings for calculated selectivities of 200 and 400 are shown as a guide. d) Isosteric heats of adsorption Q_{st} for the adsorption of CO_2, calculated using the dual-site Langmuir isotherm fits.

tion). The chlorine content of 14.42% in PPN-6-CH_2Cl was reduced to only trace amounts in the polyamine-tethered PPNs. PPN-6-CH_2DETA had the highest nitrogen content of 11.95% (see Table S5 in the Supporting Information), which corresponds to a loading of 0.3 functional groups per phenyl ring.

The introduction of polyamine groups in PPN-6 resulted in materials with excellent CO_2 adsorption characteristics at 295 K and low pressures (Figure 1b). The trend of improvement in CO_2 adsorption in terms of tethered polyamine groups was DETA > TAEA > TETA > EDA. Although PPN-6-CH_2DETA has the lowest surface area, it exhibits the highest CO_2-uptake capacity of all the polyamine-tethered PPNs. This finding indicates that the CO_2-uptake capacity is closely correlated to amine loading instead of surface area under these conditions, and the result is consistent with previous findings of Dawson et al.[8f] At 295 K and 1 bar, PPN-6-CH_2DETA exhibits exceptionally high CO_2 uptake (4.3 mmol g^{-1}, 15.8 wt%), possibly because of the accessibility of the alkylamine chain. To the best of our knowledge, this value is one of the highest of all the microporous organic polymers reported so far,[8f,9] including top-performing N-containing ones, such as N-TC-EMC[11] (4.0 mmol g^{-1}), BILP-4[12] (3.6 mmol g^{-1}), and MFB-600[13] (2.25 mmol g^{-1}).

Coal-fired power plants emit flue gas that contains approximately 15% CO_2 at total pressures of around 1 bar; thus, CO_2-uptake capacity at about 0.15 bar (partial pressure of CO_2 in flue gas) is more relevant to realistic post-combustion applications. At 295 K and 0.15 bar, PPN-6-CH_2Cl only takes up 0.25 mmol g^{-1} CO_2 (1.1 wt%), whereas PPN-6-CH_2DETA takes up 3.0 mmol g^{-1} of CO_2 (11.8 wt%). This latter value is comparable to other top-performing materials, such as mmen-CuBTTri[7] (9.5 wt% at 298 K) and MgMOF-74[14] (22.0 wt% at 293 K), but PPN-CH_2DETA stands out with respect to its physicochemical stability arising from the covalent bonding in the framework. The increase in the volumetric uptake capacity upon tethering of the polyamine chain is even more significant: from 1.3 g L^{-1} for PPN-6-CH_2Cl to 37.5 g L^{-1} for PPN-6-CH_2DETA at 295 K and 0.15 bar (the tap densities were measured to be 0.12 and 0.28 g cm^{-3} for PPN-6-CH_2Cl and PPN-6-CH_2DETA, respectively; see Table S6 and Figure S2 in the Supporting Information).

At 295 K, the polyamine-tethered PPNs adsorb less N_2 than PPN-6-CH_2Cl (see Figure S3 in the Supporting Information). PPN-6-CH_2DETA is especially interesting, with an uptake of less than 0.1 wt% N_2 at 1.0 bar, approximately one third of that of PPN-6-CH_2Cl. It is possible that the added polar sites in the former may enhance N_2 adsorption, but that this is totally offset by the significant loss of surface area. Conversely, the CO_2 uptake is significantly enhanced because the strong interactions play a more significant role.

To evaluate the CO_2/N_2 selectivity of the materials under flue-gas conditions with single-gas isotherms, we used the ideal adsorbed solution theory (IAST) model of Myers and Prausnitz[15] along with the pure component isotherm fits to determine the molar loadings in the mixture for specified partial pressures in the bulk gas phase. Figure 1c presents the component loadings of N_2 and CO_2 for PPN-6-CH_2Cl, PPN-6-CH_2EDA, PPN-6-CH_2DETA, PPN-6-SO_3Li, MgMOF-74, NaX zeolite, and mmen-CuBTTri calculated by IAST with bulk phase equilibrium partial pressures of 85 kPa (N_2) and 15 kPa (CO_2). Two factors that define a material for efficient separation of CO_2 are a high CO_2 loading and a high selectivity over N_2. Figure 1c clearly shows both factors, and highlights the high loading on PPN-6-CH_2DETA and its exceptional selectivity of CO_2 over N_2 (the better the material, the closer to the top left corner of the graph). We note that CO_2 loading is highest for MgMOF-74; however, PPN-6-CH_2DETA has a much lower N_2 uptake than MgMOF-74, thereby leading to an unprecedented selectivity compared to any reported material (see Table S7 in the Supporting Information). The poor N_2 adsorption with PPN-6-CH_2DETA can be attributed to low porosity (pore volumes are 0.573 and 0.264 $cm^3 g^{-1}$ for MgMOF-74[14] and PPN-6-CH_2DETA, respectively).

To better understand the adsorption properties, the isosteric heats of adsorption (Q_{st}) were calculated from dual-site Langmuir fits of the CO_2 isotherms at 273, 284, and 295 K. Figure 1d shows a plot of the adsorption enthalpies as a function of loading. Particularly noteworthy are the strong inflections for all the polyamine-tethered PPNs. As can be seen from Figure 1d, PPN-6-CH_2DETA retains its strong CO_2 interactions to a relatively high CO_2 loading (ca. 2.0 mmol g^{-1}), which is consistent with its large CO_2-uptake capacity. The temperatures of flue-gas streams emitted from power plants, however, are much higher than 295 K. To be practically useful for CO_2 capture under realistic flue-gas conditions, the preservation of high isosteric heats of adsorption is essential for solid adsorbents so as to maintain high CO_2-uptake capacity at elevated temperatures. Assuming full regeneration, the quantity adsorbed at 0.15 bar could be considered as the full capacity. From 295 K to 313 K, the CO_2-uptake capacity of PPN-6-CH_2DETA at 0.15 bar only dropped slightly from 11.8 to 10.0 wt% (see Figure S5 in the Supporting Information); thus, this porous material holds considerable promise for realistic post-combustion carbon-capture applications.

The advantages of solid adsorbents with high heats of adsorption include high selectivity and large CO_2 capacities at low partial pressures; however, concerns about material regeneration are often raised. To test the cyclability of PPN-6-CH_2DETA we simulated temperature and vacuum swings with an ASAP2020 analyzer, by saturating with CO_2 up to 1.1 bar at 273 K followed by a high vacuum for 100 min at 80 °C. After 20 cycles, there was no apparent loss in capacity (Figure 2), thus indicating complete desorption during each regeneration cycle. Compared to mmen-CuBTTri, PPN-6-CH_2DETA shows higher energy demands for regeneration, possibly because of the large percentage of primary amines in PPN-6-CH_2DETA as opposed to only secondary amines in mmen-CuBTTri—primary amines have been shown to form stronger bonds with CO_2. Despite the high adsorption enthalpies of these materials, the regeneration energies would still be substantially lower than for amine solutions, in which the chemisorption interactions (ca. 50–100 kJ mol^{-1}) necessitate heating the solutions containing about 70% water

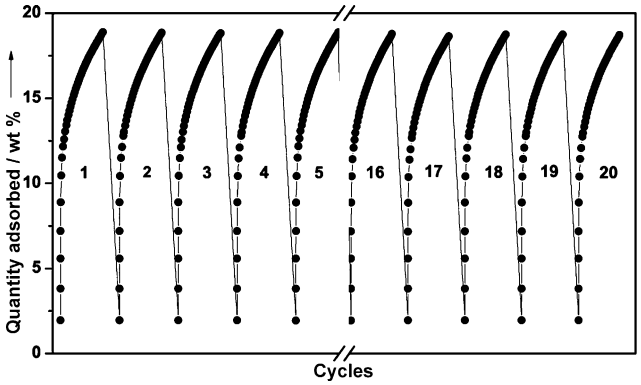

Figure 2. Twenty cycles of CO_2 uptake at 273 K. After saturation, the sample was regenerated with a temperature swing to 80 °C and then under vacuum (0.1 mmHg) for 100 min. Data were collected with an ASAP2020 analyzer.

to around 100 °C. In the latter case, the energy consumption is directly linked to the high heat capacity of water ($4.15\ J\,g^{-1}\,K^{-1}$).

Compared to aqueous alkanolamines, which not only boil-off but also degrade below 140 °C, higher decomposition temperatures were observed when these amines were fixed into PPNs. Thermogravimetric analysis (TGA) suggests polyamine-tethered PPNs to be thermally stable in air up to 200 °C (see Figure S6 in the Supporting Information).

Physicochemical stability, high CO_2 capacity, high selectivity, and low regeneration costs are the criteria by which new adsorbents for post-combustion CO_2 capture will be evaluated. The results presented herein demonstrate that aromatic chloromethylation of PPN-6 and a subsequent polyamine substitution bestows the materials with significantly enhanced CO_2-uptake capacity but much lowered N_2-uptake capacity at low pressures. PPN-6-CH_2DETA exhibits an exceptionally high binding affinity and the largest selectivity for CO_2 of any porous material reported to date. Given the outstanding physicochemical stability and mild regeneration requirements, this material has great potential for practical application in a post-combustion CO_2 capture technology.

Experimental Section

Synthesis of PPN-6: Tetrakis(4-bromophenyl)methane (205 mg, 0.32 mmol) was added to a solution of 2,2′-bipyridyl (226 mg, 1.45 mmol), bis(1,5-cyclooctadiene)nickel(0) ([Ni(cod)$_2$]; 400 mg, 1.45 mmol), and 1,5-cyclooctadiene (cod; 0.18 mL, 1.46 mmol) in anhydrous DMF/THF (30 mL/30 mL), and the mixture was stirred overnight at room temperature under argon. 6 M HCl (20 mL) was added, and the resulting mixture was stirred for 6 h. The precipitate was collected by filtration, then washed with methanol and water, and dried in vacuo to produce PPN-6 as an off-white powder (85 mg, 85 %).

Synthesis of PPN-6-CH_2Cl: A resealable flask was charged with PPN-6 (200 mg), paraformaldehyde (1.0 g), glacial AcOH (6.0 mL), H_3PO_4 (3.0 mL), and conc. HCl (20 mL). The flask was sealed and heated to 90 °C for 3 days. The resulting solid was collected, washed with water and methanol, and then dried in vacuo to produce PPN-6-CH_2Cl as a brown powder in quantitative yield.

General procedure for the introduction of polyamine groups (with the synthesis of PPN-6-CH_2DETA as an example): A resealable flask was charged with PPN-6-CH_2Cl (200 mg) and diethylenetriamine (DETA, 20 mL). The flask was sealed and heated to 90 °C for 3 days. The resulting solid was collected, washed with water and methanol, and then dried in vacuo to produce PPN-6-CH_2DETA as a brown powder in quantitative yield.

Received: March 19, 2012
Published online: June 19, 2012

Keywords: adsorption · amines · CO_2 capture · environmental chemistry · porous polymer networks

[1] a) J. D. Figueroa, T. Fout, S. Plasynski, H. McIlvried, R. D. Srivastava, *Int. J. Greenhouse Gas Control* **2008**, *2*, 9–20; b) N. MacDowell, N. Florin, A. Buchard, J. Hallett, A. Galindo, G. Jackson, C. S. Adjiman, C. K. Williams, N. Shah, P. Fennell, *Energy Environ. Sci.* **2010**, *3*, 1645–1669; c) T. Lewis, M. Faubel, B. Winter, J. C. Hemminger, *Angew. Chem.* **2011**, *123*, 10360–10363; *Angew. Chem. Int. Ed.* **2011**, *50*, 10178–10181.

[2] a) Y.-S. Bae, R. Q. Snurr, *Angew. Chem.* **2011**, *123*, 11790–11801; *Angew. Chem. Int. Ed.* **2011**, *50*, 11586–11596; b) J.-R. Li, R. J. Kuppler, H.-C. Zhou, *Chem. Soc. Rev.* **2009**, *38*, 1477–1504; c) J.-R. Li, Y. Ma, M. C. McCarthy, J. Sculley, J. Yu, H.-K. Jeong, P. B. Balbuena, H.-C. Zhou, *Coord. Chem. Rev.* **2011**, *255*, 1791–1823; d) D. M. D'Alessandro, B. Smit, J. R. Long, *Angew. Chem.* **2010**, *122*, 6194–6219; *Angew. Chem. Int. Ed.* **2010**, *49*, 6058–6082; e) Q. Wang, J. Luo, Z. Zhong, A. Borgna, *Energy Environ. Sci.* **2011**, *4*, 42–55; f) N. Hedin, L. Chen, A. Laaksonen, *Nanoscale* **2010**, *2*, 1819–1841; g) T. C. Drage, C. E. Snape, L. A. Stevens, J. Wood, J. Wang, A. I. Cooper, R. Dawson, X. Guo, C. Satterley, R. Irons, *J. Mater. Chem.* **2012**, *22*, 2815–2823.

[3] H. Furukawa, N. Ko, Y. B. Go, N. Aratani, S. B. Choi, E. Choi, A. Ö. Yazaydin, R. Q. Snurr, M. O'Keeffe, J. Kim, O. M. Yaghi, *Science* **2010**, *329*, 424–428.

[4] O. K. Farha, A. Özgür Yazaydın, I. Eryazici, C. D. Malliakas, B. G. Hauser, M. G. Kanatzidis, S. T. Nguyen, R. Q. Snurr, J. T. Hupp, *Nat. Chem.* **2010**, *2*, 944–948.

[5] D. Yuan, W. Lu, D. Zhao, H.-C. Zhou, *Adv. Mater.* **2011**, *23*, 3723–3725.

[6] a) R. Dawson, D. J. Adams, A. I. Cooper, *Chem. Sci.* **2011**, *2*, 1173–1177; b) A. Demessence, D. M. D'Alessandro, M. L. Foo, J. R. Long, *J. Am. Chem. Soc.* **2009**, *131*, 8784–8786; c) A. Torrisi, R. G. Bell, C. Mellot-Draznieks, *Cryst. Growth Des.* **2010**, *10*, 2839–2841; d) R. Babarao, S. Dai, D.-e. Jiang, *Langmuir* **2011**, *27*, 3451–3460; e) A. Thomas, *Angew. Chem.* **2010**, *122*, 8506–8523; *Angew. Chem. Int. Ed.* **2010**, *49*, 8328–8344.

[7] T. M. McDonald, D. M. D'Alessandro, R. Krishna, J. R. Long, *Chem. Sci.* **2011**, *2*, 2022–2028.

[8] a) T. Ben, H. Ren, S. Ma, D. Cao, J. Lan, X. Jing, W. Wang, J. Xu, F. Deng, J. M. Simmons, S. Qiu, G. Zhu, *Angew. Chem.* **2009**, *121*, 9621–9624; *Angew. Chem. Int. Ed.* **2009**, *48*, 9457–9460; b) W. Lu, D. Yuan, D. Zhao, C. I. Schilling, O. Plietzsch, T. Muller, S. Bräse, J. Guenther, J. Blümel, R. Krishna, Z. Li, H.-C. Zhou, *Chem. Mater.* **2010**, *22*, 5964–5972; c) J.-X. Jiang, A. Laybourn, R. Clowes, Y. Z. Khimyak, J. Bacsa, S. J. Higgins, D. J. Adams, A. I. Cooper, *Macromolecules* **2010**, *43*, 7577–7582; d) J. R. Holst, E. Stöckel, D. J. Adams, A. I. Cooper, *Macromolecules* **2010**, *43*, 8531–8538; e) J. Germain, J. M. J. Frechet, F. Svec, *Chem. Commun.* **2009**, 1526–1528; f) R. Dawson, E. Stockel, J. R. Holst, D. J. Adams, A. I. Cooper, *Energy Environ. Sci.* **2011**, *4*, 4239–4245; g) A. Trewin, A. I. Cooper, *Angew. Chem.* **2010**, *122*, 1575–1577; *Angew. Chem. Int. Ed.* **2010**, *49*, 1533–1535; h) J.-X. Jiang, F. Su, A. Trewin, C. D. Wood, N. L. Campbell, H. Niu, C. Dickinson, A. Y. Ganin, M. J. Rosseinsky, Y. Z. Khi-

myak, A. I. Cooper, *Angew. Chem.* **2007**, *119*, 8728 – 8732; *Angew. Chem. Int. Ed.* **2007**, *46*, 8574 – 8578.
[9] W. Lu, D. Yuan, J. Sculley, D. Zhao, R. Krishna, H.-C. Zhou, *J. Am. Chem. Soc.* **2011**, *133*, 18126 – 18129.
[10] J. Schmidt, M. Werner, A. Thomas, *Macromolecules* **2009**, *42*, 4426 – 4429.
[11] L. Wang, R. T. Yang, *J. Phys. Chem. C* **2012**, *116*, 1099 – 1106.
[12] M. G. Rabbani, H. M. El-Kaderi, *Chem. Mater.* **2012**, *24*, 1511 – 1517.
[13] C. Pevida, T. C. Drage, C. E. Snape, *Carbon* **2008**, *46*, 1464 – 1474.
[14] J. A. Mason, K. Sumida, Z. R. Herm, R. Krishna, J. R. Long, *Energy Environ. Sci.* **2011**, *4*, 3030 – 3040.
[15] A. L. Myers, J. M. Prausnitz, *AIChE J.* **1965**, *11*, 121 – 127.

Angewandte Chemie
Eine Zeitschrift der Gesellschaft Deutscher Chemiker

Supporting Information

69451 Weinheim, Germany

Polyamine-Tethered Porous Polymer Networks for Carbon Dioxide Capture from Flue Gas**

*Weigang Lu, Julian P. Sculley, Daqiang Yuan, Rajamani Krishna, Zhangwen Wei, and Hong-Cai Zhou**

anie_201202176_sm_miscellaneous_information.pdf

1. Materials and Methods

Solvents, reagents and chemicals were purchased from Aldrich, Alfa, and Acros. *N*,*N*-dimethylformamide (DMF) and tetrahydrofuran (THF) were dried and degassed before use. All reactions involving moisture sensitive reactants were performed under argon or nitrogen atmosphere using oven dried and/or flame dried glassware. All other solvents, reagents and chemicals were used as purchased unless stated otherwise. Nuclear magnetic resonance (NMR) data were collected on a Mercury 300 MHz NMR spectrometer. Fourier transform infrared spectroscopy (FTIR) data were collected on a SHIMADZU IRAffinity-1 FTIR Spectrophotometer. Elemental analyses (C, H, and N) were obtained from Canadian Microanalytical Service, Ltd. Thermogravimetry analyses (TGA) were performed in air on a SHIMADZU TGA-50 Thermogravimetric Analyzer, with a heating rate of 3 °C min^{-1}. The solid-state NMR spectra were measured on a *Bruker* AVANCE 400 spectrometer using densely packed powders of the PPNs in 4 mm ZrO_2 rotors. PPN-6 was synthesized as previously reported.[1]

2. Low-Pressure Sorption Measurements.

Low pressure (< 800 torr) gas sorption isotherms were measured using a Micrometrics ASAP 2020 surface area and pore size analyzer. Prior to the measurements, the samples were degassed for 10 h at 120 °C. UHP grade gases were used for all measurements. Oil-free vacuum pumps and oil-free pressure regulators were used for all measurements to prevent contamination of the samples during the degassing process and isotherm measurement. Approximately 1.0 g of sample was used for all measurements.

3. Fitting of isotherms

The measured experimental data on pure component isotherms for CO_2 and N_2, in terms of excess loadings, were first converted to absolute loading using the Peng-Robinson equation of state for estimation of the fluid densities. The pore volumes of PPN-6-CH_2Cl, PPN-6-CH_2EDA, PPN-6-CH_2TAEA, PPN-6-CH_2TETA, and PPN-6-CH_2DETA used for this purpose were 1.0184, 0.4786, 0.3382, 0.3317, and 0.2640 cm^3 g^{-1}, respectively.

The absolute component loadings were fitted with either a single-site Langmuir model or a dual-site Langmuir model, as discussed below.

For N_2 adsorption there are no discernible isotherm inflections and therefore the single-site Langmuir model

$$q = \frac{q_{sat} bp}{1 + bp} \tag{1}$$

was used for fitting of the 295 K isotherms for three structures. The single-site Langmuir fit parameters are specified in Table S0.

For CO_2 adsorption in PPN-6-CH_2Cl there are also no discernible isotherm inflections and therefore the single-site Langmuir model is adequate. The isotherm data measured at 273 K, 284 K, and 295 K were all fitted with the temperature dependence of the Langmuir constant, *b*, expressed as

$$b = b_0 \exp\left(\frac{E}{RT}\right) \tag{2}$$

The parameters for the single-site Langmuir fits are specified in Table S0.

For adsorption of CO_2 in polyamine-tethered PPNs, there are subtle isotherm inflections and for fitting the experimental data we used the dual-site Langmuir model

$$q \equiv q_A + q_B = \frac{q_{sat,A} b_A p}{1 + b_A p} + \frac{q_{sat,B} b_B p}{1 + b_B p} \tag{3}$$

where we have two distinct adsorption sites A and B. The temperature dependence of the Langmuir constants for each of these sites is described by equation (2). The dual-site Langmuir parameters used for fitting the isotherm data at 273 K, 284 K, and 295 K specified in Table S0, and S0, for polyamine-tethered PPNs respectively.

4. Isosteric heats of adsorption

For CO_2 adsorption in PPN-6-CH_2Cl and polyamine-tethered PPNs, the isosteric heat of adsorption, Q_{st}, were calculated using

$$Q_{st} = RT^2 \left(\frac{\partial \ln p}{\partial T}\right)_q \tag{4}$$

The details of the analytic procedure adopted for determining Q_{st} for the dual-site Langmuir model are provided in the Electronic Supplementary Information accompanying the paper Mason et al.[2]

5. IAST calculations of loadings for mixture adsorption

In order to compare the efficacy of polyamine-tethered PPNs for CO_2/N_2 separation, we used the Ideal Adsorbed Solution Theory (IAST) of Myers and Prausnitz[3] along with the pure component isotherm fits to determine the molar loadings in the mixture for specified partial pressures in the bulk gas phase.

Notation

b	parameter in the pure component Langmuir adsorption isotherm, Pa^{-1}
$-E$	heat of adsorption, J mol^{-1}
L	length of packed bed adsorber, m
p	bulk gas phase pressure, Pa
q	molar loading of adsorbate, mol kg^{-1}
q_{sat}	saturation loading, mol kg^{-1}
Q_{st}	isosteric heat of adsorption, J mol^{-1}
R	gas constant, 8.314 J mol^{-1} K^{-1}
t	time, s
T	temperature, K
u	superficial gas velocity, m s^{-1}

Greek letters

ε	voidage of packed bed, dimensionless
ρ	framework density, kg m^{-3}
τ	time, dimensionless
τ_{break}	breakthrough time, dimensionless

Subscripts

A	referring to site A
B	referring to site A
sat	referring to saturation conditions

Table S1. Single-site Langmuir parameters for adsorption of N_2. These parameters were determined by fitting adsorption isotherms at 295 K.

	$q_{sat,A}$ mol kg^{-1}	b_A Pa^{-1}
PPN-6-CH_2Cl	0.63	2.8×10^{-6}
PPN-6-CH_2EDA	0.33	4.565×10^{-6}
PPN-6-CH_2DETA	0.1	7.647×10^{-6}

$$q = \frac{q_{sat} b p}{1 + b p}$$

$$q_{sat} = 5 \text{ mol kg}^{-1}$$

$$b = b_0 \exp\left(\frac{E}{RT}\right);$$

$$b_0 = 5.06\times10^{-10} \text{ Pa}^{-1}$$

$$E = 15 \text{ kJ mol}^{-1}$$

Table S2. Single-site Langmuir parameters for adsorption of CO_2 in PPN-6-CH_2Cl. These parameters were determined by fitting adsorption isotherms for temperatures 273 K, 284 K, and 295 K.

$$q = \frac{q_{sat} b p}{1 + b p}$$

$$q_{sat} = 10.4 \text{ mol kg}^{-1}$$

$$b = b_0 \exp\left(\frac{E}{RT}\right);$$

$$b_0 = 3.81\times10^{-10} \text{ Pa}^{-1}$$

$$E = 20.6 \text{ kJ mol}^{-1}$$

Table S3. Dual-site Langmuir parameter for adsorption of CO_2 in PPN-6-CH_2EDA. These parameters were determined by fitting adsorption isotherms for temperatures 273 K, 284 K, and 295 K.

$$q \equiv q_A + q_B = \frac{q_{sat,A} b_A p}{1 + b_A p} + \frac{q_{sat,B} b_B p}{1 + b_B p}$$

$q_{sat,A} = 1.42 \text{ mol kg}^{-1}$

$q_{sat,B} = 4.8 \text{ mol kg}^{-1}$

$b_A = b_{A0} \exp\left(\frac{E_A}{RT}\right);$

$b_{A0} = 2.55\times10^{-13} \text{ Pa}^{-1}$

$E_A = 56 \text{ kJ mol}^{-1}$

$b_B = b_{B0} \exp\left(\frac{E_B}{RT}\right);$

$b_{B0} = 6.54\times10^{-12} \text{ Pa}^{-1}$

$E_B = 34 \text{ kJ mol}^{-1}$

Table S4. Dual-site Langmuir parameter for adsorption of CO_2 in PPN-6-CH_2DETA. These parameters were determined by fitting adsorption isotherms for temperatures 273 K, 284 K, and 295 K.

$$q \equiv q_A + q_B = \frac{q_{sat,A} b_A p}{1 + b_A p} + \frac{q_{sat,B} b_B p}{1 + b_B p}$$

$q_{sat,A} = 2.35 \text{ mol kg}^{-1}$

$q_{sat,B} = 3 \text{ mol kg}^{-1}$

$b_A = b_{A0} \exp\left(\frac{E_A}{RT}\right);$

$b_{A0} = 2.94\times10^{-12} \text{ Pa}^{-1}$

$E_A = 56 \text{ kJ mol}^{-1}$

$b_B = b_{B0} \exp\left(\frac{E_B}{RT}\right);$

$b_{B0} = 5.66\times10^{-12} \text{ Pa}^{-1}$

$E_B = 37 \text{ kJ mol}^{-1}$

Table S5. Elemental Analysis data

	PPN-6-CH_2Cl	PPN-6-CH_2EDA	PPN-6-CH_2TAEA	PPN-6-CH_2TETA	PPN-6-CH_2DETA
Cl%	14.42	0.33	< 0.25	< 0.25	< 0.25
N%	0.0	7.53	9.31	9.04	11.95

* Dried at 100 °C under vacuum for 10 hours before measurement.

** Measured by Atlantic Microlab, Inc.

*** Data is average of two measurements.

Table S6 Tap density

PPN-6-CH_2Cl	PPN-6-CH_2EDA	PPN-6-CH_2TAEA	PPN-6-CH_2TETA	PPN-6-CH_2DETA
0.12	0.24	0.23	0.22	0.28

* Data is average of ten measurements, STDev's less than 0.01 g/ml.

Table S7 IAST calculated adsorption selectivity

Materials	CO_2 loading at 15 kPa mol/kg	N_2 loading at 85 kPa mol/kg	Selectivity* $S=(q_1/q_2)/(p_1/p_2)$
MgMOF-74	6.4367	0.18725	195
NaX Zeolite	3.0316	0.10192	169
mmen-CuBTTri	2.2241	0.038312	329
PPN-6-CH_2Cl	0.2336	0.1012	13
PPN-6-CH_2EDA	1.82	0.09	115
PPN-6-CH_2DETA	3.04	0.039	442
PPN-6-SO_3Li	1.244	0.017	415

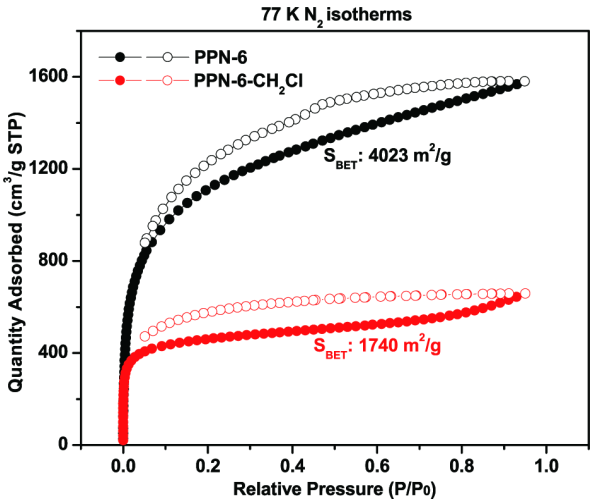

Figure S1.77 K N_2 isotherms of PPN-6 and PPN-6-CH_2Cl, adsorption (●)/desorption (○).

Figure S2.Tap density measurement demonstration.

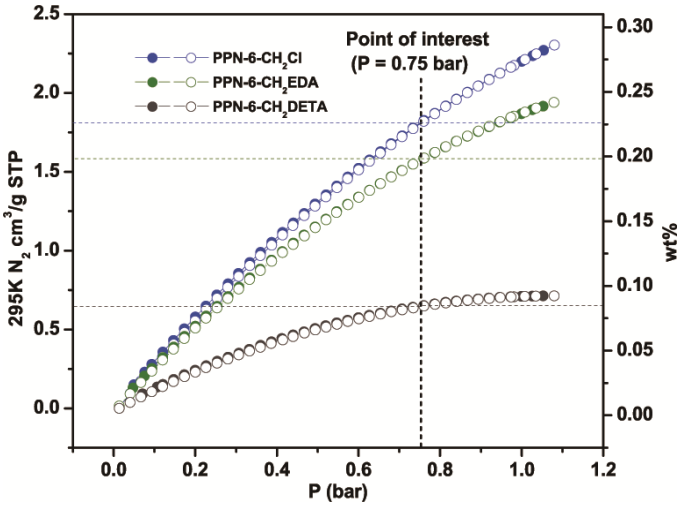

Figure S3. 295 K N_2 sorption isotherms, adsorption (●)/desorption (○), *ca*. 1.0 g of each sample and filling rod was used for measurement.

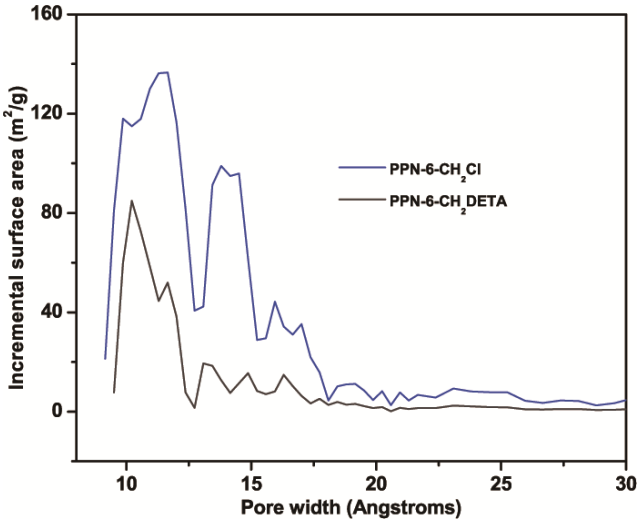

Figure S4. Pore size distribution curves of PPN-6-CH_2Cl (blue) and PPN-6-CH_2DETA (gray).

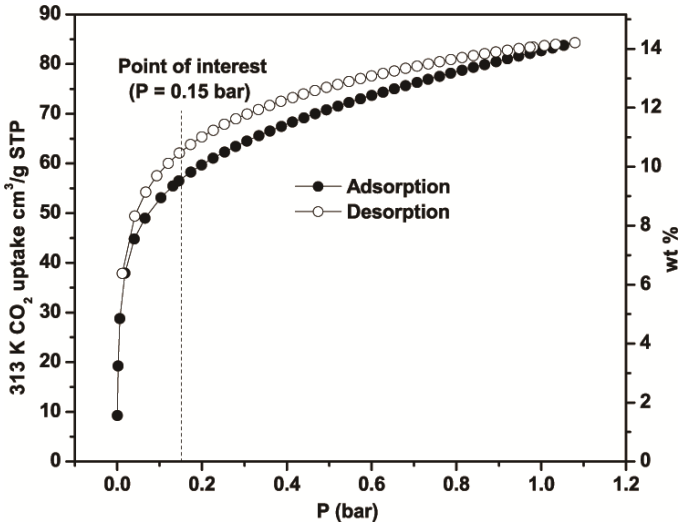

Figure S5. 313 K CO_2 sorption isotherms of PPN-6-CH_2DETA, adsorption (●)/desorption (○).

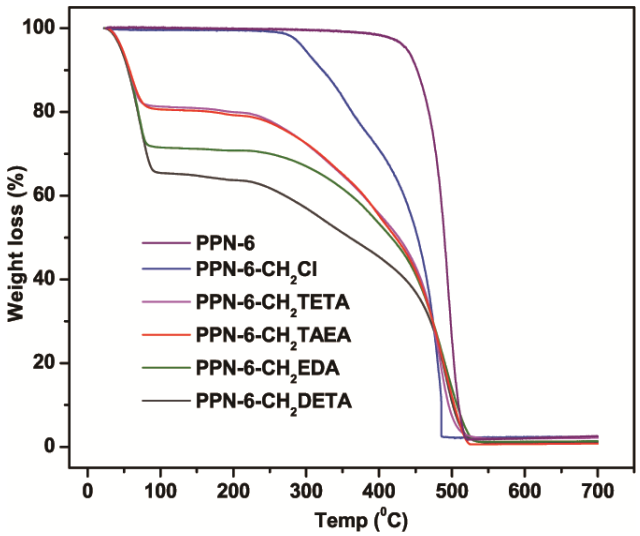

Figure S6. Thermogravimetric data.

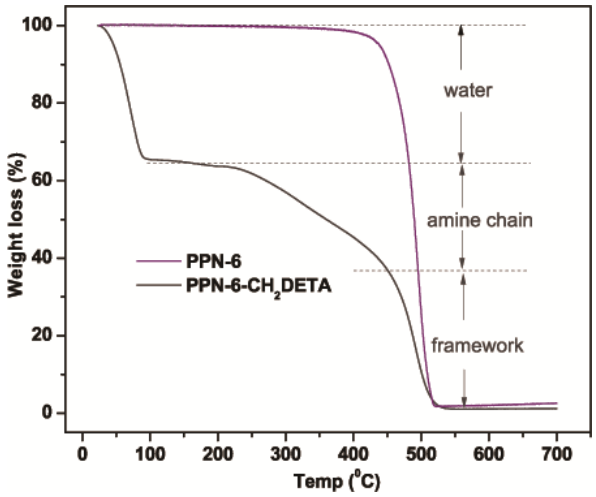

Figure S7. Thermogravimetric data of PPN-6-CH_2DETA with proposed weight loss.

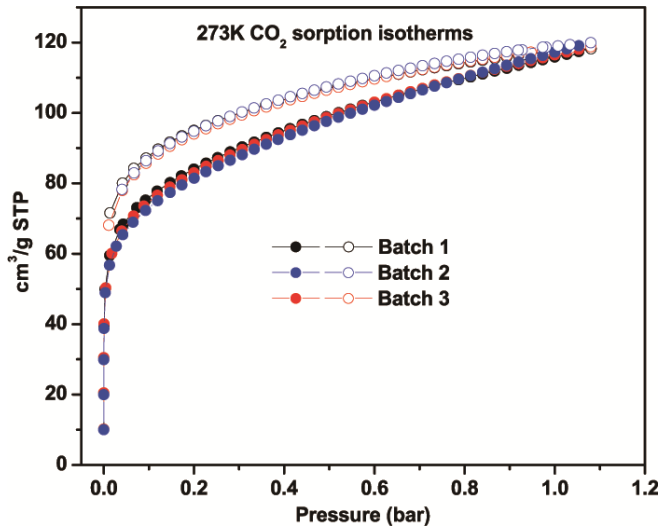

Figure S8. Reproducibility of PPN-6-CH_2DETA.

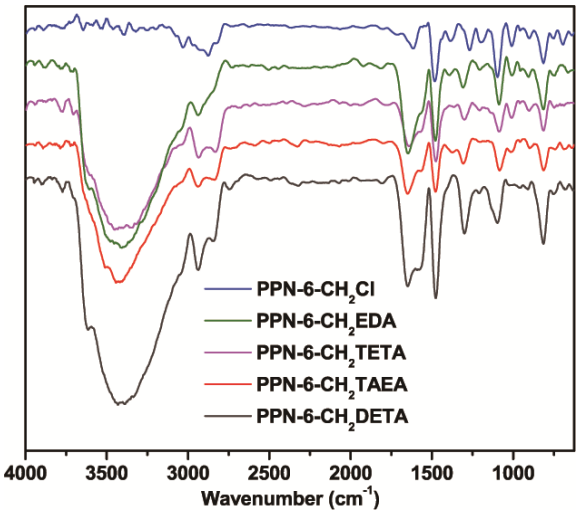

Figure S9. FT-IR spectra.

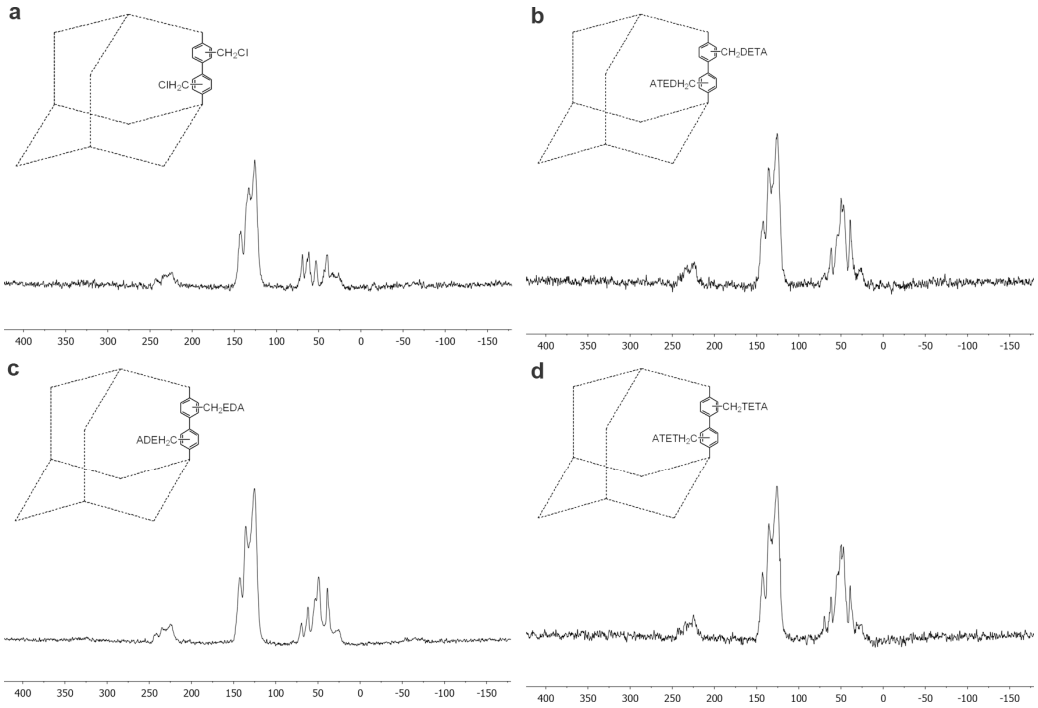

Figure S10. ^{13}C CP/MAS NMR spectrum (4mm, Bybass, 10KHz, Field = -2000, p15 = 2000).

References

[1] W. Lu, D. Yuan, J. Sculley, D. Zhao, R. Krishna, H.-C. Zhou, *J. Am. Chem. Soc.* **2011**, *133*, 18126-18129.

[2] J. A. Mason, K. Sumida, Z. R. Herm, R. Krishna, J. R. Long, *Energy Environ. Sci.* **2011**, *4*, 3030-3040.

[3] A. L. Myers, J. M. Prausnitz, *A.I.Ch.E.J.* **1965**, *11*, 121-130.